Journal of the Physical Society of Japan **92**, 024601 (2023)
https://doi.org/10.7566/JPSJ.92.024601

Heat-flux-driven Rotation of Cholesteric Droplets Dispersed in Glycerol

Shunsuke Takano[1], Shinji Bono[1,2], and Yuka Tabe[1,3*]

[1]*Faulty of Science and Engineering, Waseda University, Shinjuku, Tokyo 169-8555, Japan*
[2]*College of Science and Engineering, Ritsumeikan University, Shiga 525-8577, Japan*
[3]*Kagami Memorial Research Institute for Materials Science and Technology, Shinjuku, Tokyo 169-0051, Japan*

(Received November 9, 2022; accepted December 8, 2022; published online January 17, 2023)

Micron-sized cholesteric droplets dispersed in glycerol exhibit steady rigid rotation under a uniform temperature gradient about the axis parallel to the gradient. The rotational velocity is linear to the temperature gradient, and the chirality inversion reverses the rotational direction. The result clearly contrasts previous studies showing that cholesteric droplets in immiscible liquids such as glycerol and water never rotated under a temperature gradient. We demonstrated the steady and continuous rotation of the cholesteric droplets driven by a heat flux by hydrophilizing the substrate surface to adsorb the glycerol molecules. The thermomechanical coupling constant was found to be $|\nu| \geq 3 \times 10^{-7}\,\mathrm{N\,m^{-1}\,K^{-1}}$.

1. Introduction

When a droplet composed of chiral liquid crystals (LCs) is subjected to a temperature gradient, it exhibits unidirectional steady rotation about the axis parallel to a heat flux.[1–5] The "Lehmann effect" phenomenon was first reported by O. Lehmann in 1900 and has been known as a unique thermomechanical coupling in chiral LCs. Recently, the Lehmann effect has been refocused as a candidate for active soft matter since it can directly transform a heat flux into angular momentum of chiral LCs. So far, the Lehmann effect has been mostly studied in the following two systems; one is that cholesteric (Ch) droplets coexist with their own isotropic phase,[2–6] and the other is that droplets are dispersed in partially miscible liquids.[1,7–10] In comparison, the latter has the advantage that the operating temperature region is wide and flexible, enabling us to easily conduct experiments and develop the system into future applications. However, one concern has been suggested about the driving force: the rotation of the droplets in the partially miscible liquids should not be driven by the heat flux.[8] The previous studies reported that the Ch droplets in immiscible liquids such as water and glycerol never rotated under a temperature gradient.[7,8] In contrast, the same droplets dispersed in partially miscible liquids exhibited steady rotations.[7,8] It was shown that what drives the rotation of the droplets was not the heat flux but Marangoni convection and/or the accompanied mass fluxes.[7,8] The experimental facts raised the question of whether no torque was induced by the temperature gradient when the Ch droplets were suspended in immiscible liquids, or whether a certain resistant torque disturbed their rotations. Theoretically, when Ch LC is subjected to a temperature gradient ∇T, director $\boldsymbol{n}$ is supposed to be subjected to the thermomechanical torque $\boldsymbol{\tau}$, which is described by Leslie's phenomenological equation as[11]

$$\boldsymbol{\tau} = \nu \boldsymbol{n} \times (\boldsymbol{n} \times (-\nabla T)). \tag{1}$$

Here, ν is the thermomechanical coupling constant, the sign of which is reversed by changing the chirality of the LC sample. This non-trivial cross-coupling is expected to exist in all chiral LCs with broken mirror symmetry, including the Ch droplets in water and glycerol. It should be clarified why the Ch droplets never rotated in immiscible liquids to understand the rotational mechanism of the Ch droplets and for its future application.

In this report, we dispersed micron-sized Ch droplets in glycerol and applied a uniform temperature gradient to the emulsions. If Eq. (1) is applied to our system, the torque exerted on the droplets should change its sign when either the chirality or the direction of the temperature gradient is reversed. Also, the torque magnitude is expected to be linear to the absolute temperature gradient value. Checking these properties one by one, we examined the motion of the Ch droplets in glycerol.

2. Experimental

2.1 Sample preparation

An LC sample was prepared by adding the chiral compound of (R)-2-Octyl 4-[4-(Hexyloxy)benzoyloxy]benzoate [(R)-dopant, from TCI] to the host nematic RDP-V0639 (from DIC) at a concentration of ∼1 wt %. The mixture was manually stirred into glycerol with a normal purity of 99.7% (from Sigma-Aldrich) with a volume ratio of 1 : 100. The Ch compound was dispersed in glycerol without additional surfactants, forming micron-sized droplets. An enantiomeric sample composed of RDP-V0639 and (S)-2-Octyl 4-[4-(Hexyloxy)benzoyloxy]benzoate [(S)-dopant] was prepared by the same procedure. The phase sequences of the LC samples with (R)- and (S)-dopants were Ch|74.8 °C|Ch+Iso|76.7 °C|Iso and Ch|74.6 °C|Ch+Iso|76.4 °C|Iso, respectively. In the Particle Tracking Velocimetry (PTV) experiment, synthetic resin beads with 2.5 µm diameters, named Ex-0025 (from Sekisui Chemical), were added to the emulsions as tracer particles. All the experiments were conducted in the cholesteric temperature region.

An emulsion sample was sandwiched between a slide glass (1.3 mm thickness) and a cover glass (0.15 mm thickness), the distance between which was adjusted to 100 µm using a polyester film spacer (from Toray Industries). To hydrophilize the surface, the glasses were (1) ultrasonically washed in an alkaline detergent solution, (2) rinsed with tap water, (3) ultrasonically washed in distilled water, and (4) irradiated with UV rays in an ozone atmosphere.

2.2 Observation under a heat flux

The experimental setup is shown in Fig. 1. The temperatures of the upper and the lower sides of a sample cell were adjusted with the temperature controllers of TS62–STC200 and TS62–mK2000 (from Instec), respectively, providing a uniform temperature gradient perpendicular to the substrates.

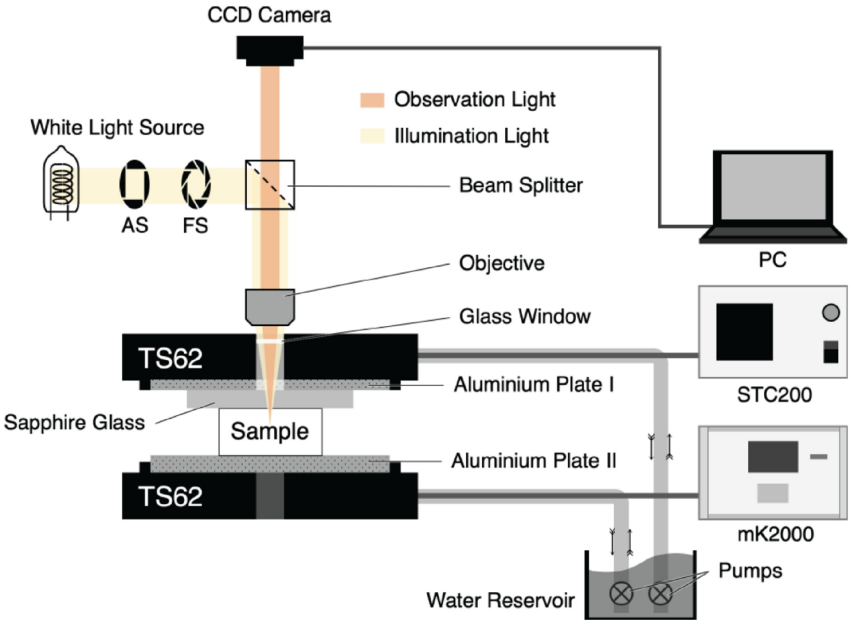

Fig. 1. (Color online) Schematic figure of the experimental setup. The sample was sandwiched by two thermal control stages, TS62 (Instec), through which the temperature and its gradient were controlled. Samples were observed by a reflected light microscope.

In this paper, when the upper temperature was higher than the lower, the temperature gradient sign was defined to be positive (+) and called an upward gradient, and vice versa.

We used a reflected light microscope, BX51-BXRLA2 (from Olympus), to observe the emulsion samples and took images and movies with a CCD camera, DFK 23U445 (from The Imaging Source Asia). The three-dimensional analysis of the 100 µm-thickness samples was performed using a C2 confocal microscope system with an upright Eclipse Ni (Nikon) in the reflection mode with a 561-nm laser beam.

3. Results and Discussion

3.1 Textures of Ch droplets dispersed in glycerol

In the emulsion samples, the Ch compounds were dispersed in glycerol confined to spherical droplets (hereafter called Ch droplets) with a radius of 1–50 µm. Since the density of the Ch compounds is lower than that of glycerol (∼4 : 5), the Ch droplets were positioned near the upper substrate. Due to the spatial confinement and the planar degenerating anchoring at the Ch-glycerol interface, the droplets took several frustrated molecular alignment types, depending on the size relative to the cholesteric pitch.[12] Figure 2(a) shows the most frequently observed texture under an optical microscope, called radial spherical structure (RSS). The detailed director orientation was described in the previous works.[12,13] The RSS was characterized by a double helix of cholesteric disclinations extending from the droplet center to the surface, along which it possessed twofold symmetry. When the microscope illumination was incident along the symmetry axis, the RSS droplet exhibited the double spiral pattern, as shown in Fig. 2(a). The width of the stripes corresponded to the half pitch of the Ch, which was ∼4 µm. The next frequently observed texture is shown in Fig. 2(b) (the larger droplet) and in Fig. 2(c), which are called diametrical spherical structures (DSS).[12] The DSS was composed of the curved Ch layers normal to the radial direction accompanied by a diametrical array of defect rings, about which the DSS possessed cylindrical symmetry. The detailed director orientation is given in Refs. 12 and 13. When a DSS droplet was observed by optical microscopy, the textural symmetry depended on the angle between the cylindrical axis and the incident light direction due to the cylindrical structure. If the cylindrical axis was parallel to the incident light (perpendicular to the paper plane), one could observe the texture shown in Fig. 2(b) (the larger droplet) and in the leftmost micrograph of Fig. 2(c). In Fig. 2(c), the cylindrical axis gradually tilted from the incident light direction from left to right and eventually became perpendicular to that. Corresponding to this motion, the twofold symmetry in the leftmost texture was transformed into the infinite symmetry in the rightmost one. Although RSS should have the lowest free energy in the present condition,[12,13] both the RSS and the DSS droplets were stable enough to survive for several tens of hours.

3.2 Rotation of Ch droplets subjected to a temperature gradient in glycerol

Both RSS and DSS droplets suspended in glycerol exhibited a steady unidirectional rotation when subjected to a uniform temperature gradient. As shown in Fig. 2(a), when the temperature gradient was applied in the upward direction (from the back to the front of the paper), the RSS droplet containing (R)-dopant rotated its spiral texture in the anticlockwise direction (see also Movie 2a[14]). When the chirality of the dopant was inversed, the rotational direction was reversed. In the sequence of micrographs of Fig. 2(b) (also in Movie 2b[15]), the large DSS droplet and the small RSS droplet containing (S)-dopant exhibited the clockwise rotation under the upward temperature gradient. On the other hand, the DSS droplets in Fig. 2(c) and in Movie 2c[16] showed no textural rotation when the cylindrical axis was parallel to the temperature gradient. It means that the pure director rotation did not occur in this geometry, but it was not

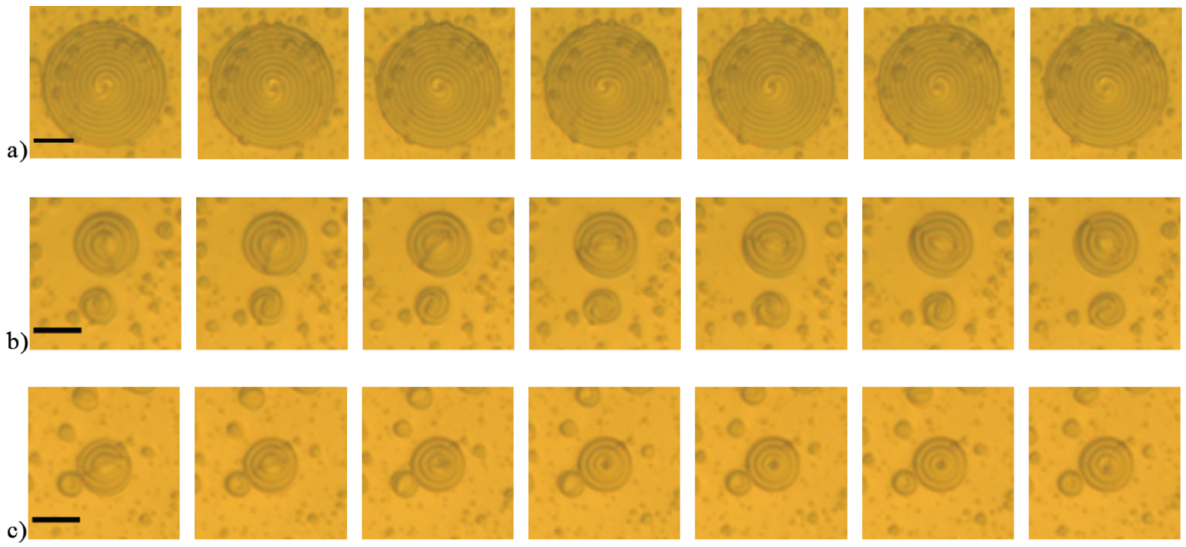

Fig. 2. (Color online) Textures of Ch droplets dispersed in glycerol and their time evolution under a temperature gradient. The images were taken every 180 s under the reflected light microscope. The scale bars indicate 20 μm. (a) An RSS droplet containing (R)-dopant with the disclination lines perpendicular to the paper. The central temperature of the sample, T_c, was set at 61.6 °C and the temperature gradient, ∇T, was +10.0 mK μm^{-1} (the heat flows from the front to the rear sides of the paper). See also Movie 2a. (b) An RSS droplet (the smaller one) and a DSS droplet (the larger one), containing (S)-dopant. The disclination line (cylindrical axis) of the DSS droplet is in the direction parallel to the paper surface. T_c = 61.6 °C and ∇T = +20.0 mK μm^{-1}. See also Movie 2b. (c) A DSS droplet with (R)-dopant. The cylindrical axis changed the direction from parallel (leftmost) to perpendicular (rightmost) relative to the paper plane. The central temperature and the temperature gradient were T_c = 61.6 °C and ∇T = −20.0 mK μm^{-1}, respectively. See Movie 2c.

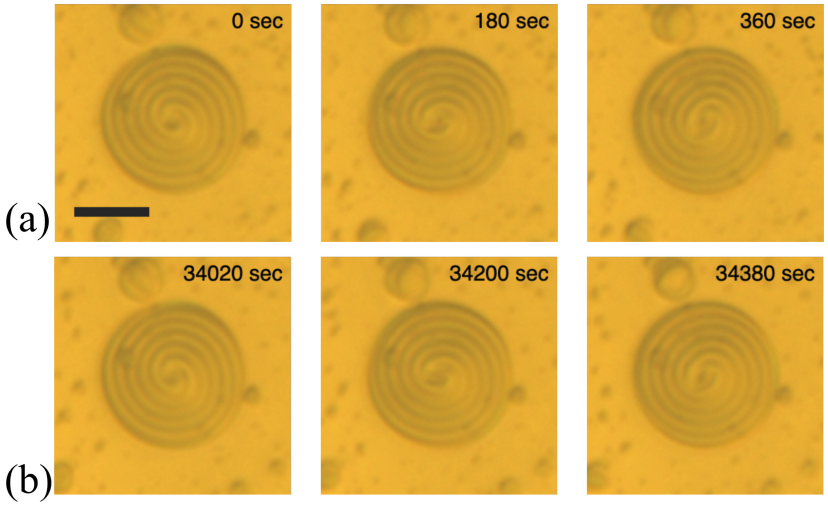

Fig. 3. (Color online) Time evolution of an RSS droplet with (R)-dopant. The temperature gradient was ∇T = +10.0 mK μm^{-1}, and the central temperature was T_c = 61.6 °C. The scale bar is 20 μm. During the total observation time of 9 h, (a) the micrographs taken at t = 0, 180, and 360 s (from the left to the right) and (b) at t = 9 h 27 min + 0 s, 180 s, and 360 s (from the left to the right).

impossible for the droplet to rotate as a rigid body, which the optical microscope could not determine.

In the following subsections, for simplicity, we focused on the RSS droplets and examined their motion in detail.

3.2.1 *Stability of rotation*

The motion of an RSS droplet under a temperature gradient of +10.0 mK μm^{-1} was tracked for about 9.6 h. The result is shown in the consecutive micrographs of Fig. 3. The droplet containing (R)-dopant exhibited continuous anticlockwise textural rotations under the upward temperature gradient over the observation period. The rotational velocity was measured as follows: taking the polar coordinate with the origin located at the droplet center, we tracked the angle of an arbitrary point in the droplet from the initial position. As shown in Fig. 4, the angle increased at the constant rate of 4.3×10^{-3} rad s^{-1} for the entire observation period of 9.6 h, proving the steady and continuous rotation of the Ch droplets under the temperature gradient.

3.2.2 *Rotational direction of Ch droplets: dependence on chirality and heat flux direction*

We dispersed Ch droplets containing (R)-dopant [called (R)-droplets] and (S)-dopant [called (S)-droplets] in glycerol and applied a temperature gradient in the upward or downward direction to each to examine the dependence of the rotational velocity on the chirality of the samples. The result is summarized in Fig. 5 and Movies 5a–5d.[17–20] As shown in the sequence of micrographs at the upper left of Fig. 5, the (R)-droplet exhibited the anticlockwise rotation

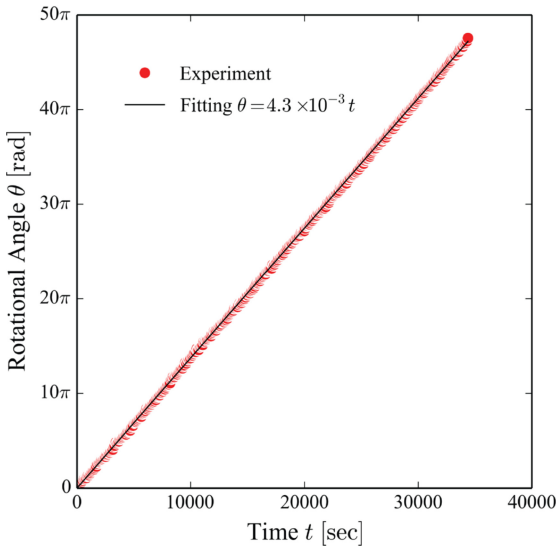

Fig. 4. (Color online) Time evolution of the angle of an arbitrary point of the RSS droplet in Fig. 3 from the initial angle.

under the upward temperature gradient. When either the chirality or the temperature gradient direction was reversed, the rotational direction was reversed. If both were changed, the (S)-droplet under the downward temperature gradient rotated in the same direction as the (R)-droplet under the upward gradient. The rotational velocity magnitude was nearly the same for all four droplets possessing the same size under the same $|\nabla T|$.

3.2.3 *Dependence of rotational velocity on the temperature gradient magnitude*

Next, the dependence of the rotational velocity of the Ch droplets, ω, on the temperature gradient, ∇T, was examined quantitatively. First, ∇T was step-wisely changed, and the motion of an arbitrary point in an (R)-droplet was tracked. The result is shown in Fig. 6. In the period of $T = 0$–2700 s, the temperature gradient was fixed at $\nabla T = +20\,\mathrm{mK\,\mu m^{-1}}$, and the (R)-droplet rotated in the anticlockwise direction at the constant angular velocity of $\omega \sim 2.7\pi \times 10^{-3}\,\mathrm{rad\,s^{-1}}$. At $T = 2700$ s, ∇T was abruptly changed to $+10\,\mathrm{mK\,\mu m^{-1}}$, and then ω dropped down to $\sim 1.35\pi \times 10^{-3}\,\mathrm{rad\,s^{-1}}$. When ∇T

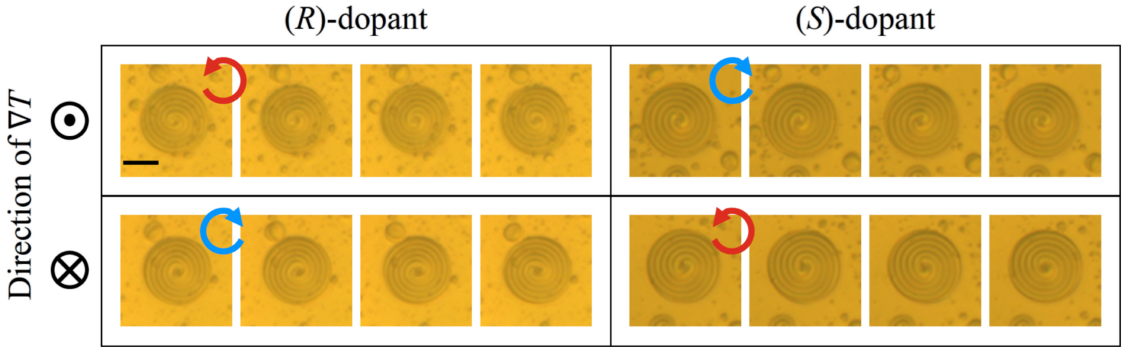

Fig. 5. (Color online) RSS droplets with (R)- and (S)-dopants, under the upward and downward temperature gradients, respectively. The central temperature was set at $T_c = 61.6\,^\circ$C. In the upper and lower rows, the temperature gradients applied to the droplets were $\nabla T = +10.0$ and $-10.0\,\mathrm{mK\,\mu m^{-1}}$, respectively. The sequential micrographs of each droplet were taken at 180 s intervals. The scale bar indicates 20 µm. The videos corresponding to the images in the upper left, the lower left, the upper right and the lower right are Movies 5a, 5b, 5c, and 5d, respectively.

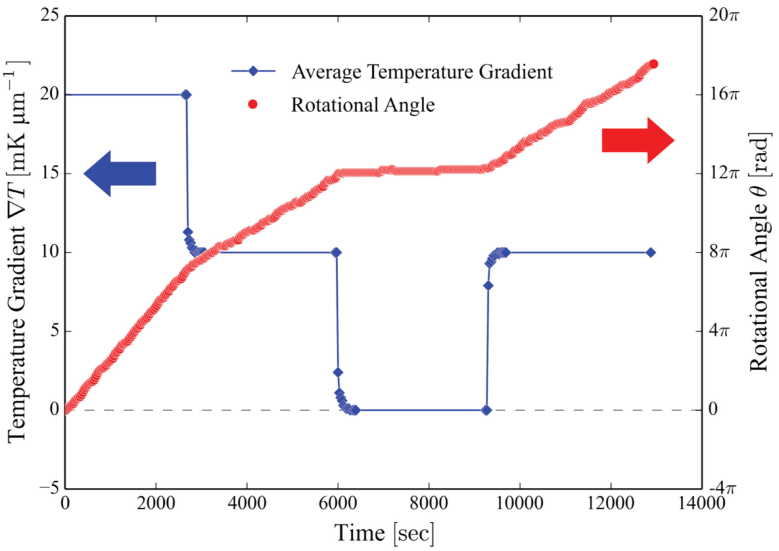

Fig. 6. (Color online) Response of the rotation angle of an (R)-RSS droplet to the stepwise change of the temperature gradient. The temperature gradient and the rotation angle are plotted on the left and right vertical axes, respectively. Note that just after the temperature change, the exact value of ∇T inside the droplet might be slightly deviated from the average value given in the figure.

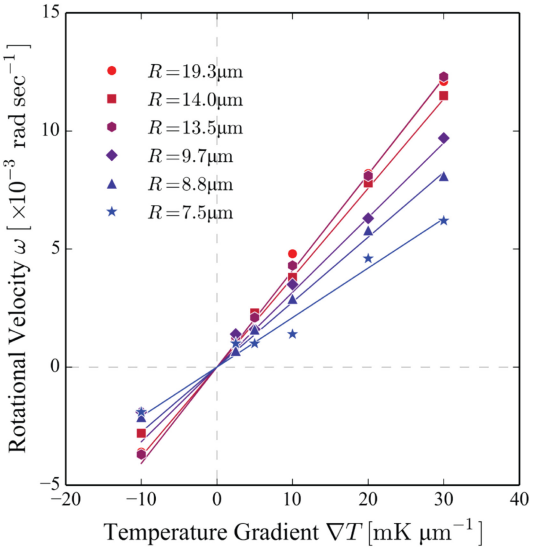

Fig. 7. (Color online) Dependence of the rotational velocity of (R)-RSS droplets with various sizes on the temperature gradient.

was set to zero at $T = 6300$ s, the droplet stopped the rotation and remained at rest. At $T = 9600$ s, ∇T was step-wisely increased to $+10\,\mathrm{mK\,\mu m^{-1}}$, which restarted the rotation of the droplet with a velocity of $\sim 1.35\pi \times 10^{-3}\,\mathrm{rad\,s^{-1}}$.

We tracked the motion of (R)-droplets with various sizes and examined the relation between ∇T and ω, and obtained Fig. 7. Obviously, the linear dependence was satisfied with each droplet. Figure 7 also suggests that the larger droplets tended to rotate faster, though the dependence was not simply monotonic. Due to the individual differences and the complexity, the relation between ω and the droplet size cannot be further discussed here. Nevertheless, it was clearly proved that ω was always linear to ∇T for the various-sized droplets.

3.3 *Rigid-body rotation of Ch droplets*

The textural rotation of the Ch droplets observed by the optical microscope should result from the following two independent molecular motions or their combination, i.e., the director rotation inside each droplet and the rigid body rotation as a whole droplet. Since the optical microscope cannot distinguish the two motions, we used the PTV method to reveal the meaning of the textural rotation. When a small amount of resin beads was added to an emulsion, some adhered to the surfaces of the Ch droplets, the motion of which visualized the hydrodynamic flow in the droplets. The result is shown in Fig. 8 and Movies 8a–8c.[21–23] In Figs. 8(a) and 8(b), the beads attached to the (R)-droplets exhibited the anticlockwise rotation about the center of the droplets under the upward temperature gradient. In Fig. 8(c), the bead adhered to the (S)-droplet and rotated in the clockwise direction about the droplet center. In each, the angular velocity of the beads was the same as the velocity of the textural rotation. It should be noted that the beads were not trapped by the disclinations but could adhere to any points of the surfaces, and no apparent orientational distortion was observed in their vicinity. The agreement between the angular velocities of the beads and that of the textural rotation indicates that the Ch droplets should have rotated as rigid bodies. As noticed in Fig. 8, the beads never moved in the direction parallel to the temperature gradient, suggesting the absence of Marangoni convection. Indeed, it has been reported that[8] the interfacial tension between Ch LCs and glycerol does not depend on temperature; therefore, no Marangoni convection should exist in the droplets. The motion of the tracer particles is consistent with the report.

3.4 *Positions of Ch droplets with respect to the upper substrate*

In emulsion cells, the Ch droplets were distributed in the vicinity of the upper substrate because their density was lower than glycerol. Despite the buoyancy, many of the droplets showed vigorous Brownian motion in the equilibrium, indicating that they did not adhere to the substrate. It should result from the high hydrophilicity of the substrate

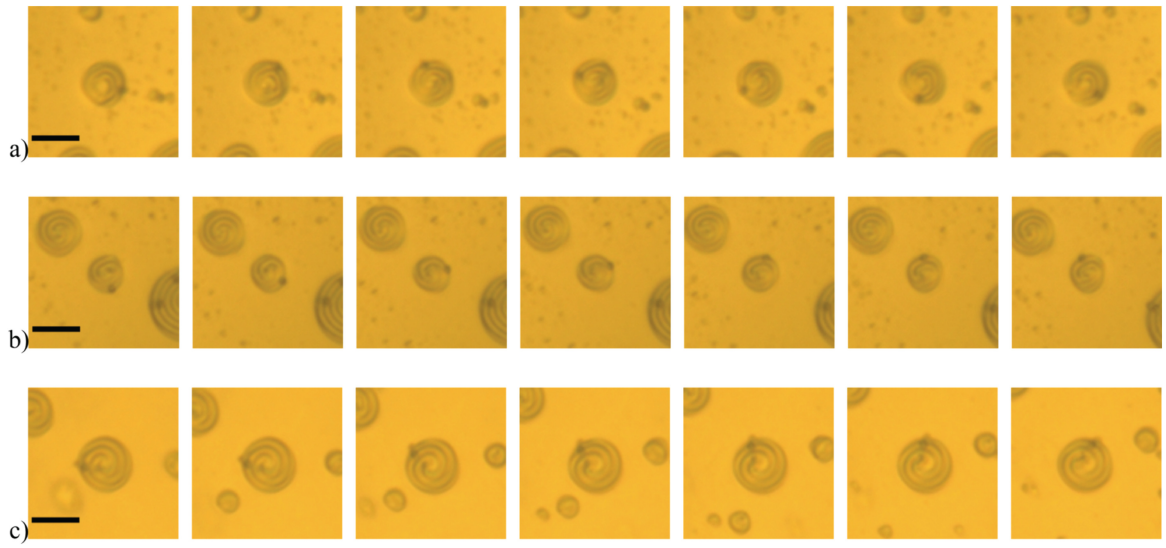

Fig. 8. (Color online) Sequences of micrographs of the RSS droplets with the marker particles attached. The images were taken under a reflected light microscope at 90 s intervals. The central temperature was set at $T_c = 61.6\,^{\circ}\mathrm{C}$. The scale bar is 20 μm. (a) The droplet containing (R)-dopant under $\nabla T = +20.0\,\mathrm{mK\,\mu m^{-1}}$; the images were exported from Movie 8a, (b) the droplet with (R)-dopant under $\nabla T = +10.0\,\mathrm{mK\,\mu m^{-1}}$, exported from Movie 8b, (c) the droplet with (S)-dopant under $\nabla T = +20.0\,\mathrm{mK\,\mu m^{-1}}$, exported from Movie 8c.

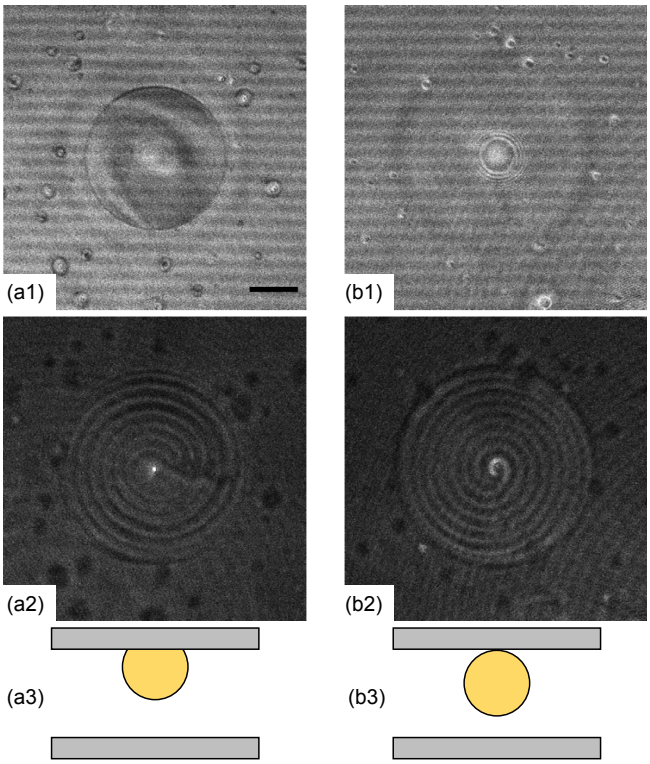

Fig. 9. (Color online) (a1)–(b2) Confocal reflective microscopy images of RSS droplets dispersed in glycerol. The scale bar indicates 20 μm. The upper row: the cross-section images of the interface between the droplets and the upper substrate. The lower row: the cross-section images of the droplets 13 μm below the upper substrate surface. (a1, a2) the droplet without thermal fluctuation; (b1, b2) the droplet with Brownian motion. (a3, b3) the schematic figures showing the positions of the droplets with respect to the substrate.

surface, on which the glycerol molecules were adsorbed and played the role of lubricant. To confirm that, we used confocal microscopy and examined the vertical positions of two droplets, one of which showed no thermal fluctuation, and the other performed Brownian motion in the equilibrium. Figures 9(a1)–9(b2) show their cross sections, just below the upper substrate (a1, b1) and 13 μm below that (a2, b2), respectively. Both droplets were positioned near the substrate, but there was a crucial difference between them. In Fig. 9(a1), a clear circular line is noticed, inside which all the area was in focus and the reflectivity was higher than the outside. This micrograph suggests that the droplet should have been brought into surface contact with the upper substrate, with a radius of ∼29 μm, as schematically depicted in Fig. 9(a3). In Fig. 9(b1), in contrast, no such circular line was observed except for the interference fringe caused by an optical artifact, indicating that the droplet did not adhere to the substrate as shown in Fig. 9(b3). The adhering condition observed in Fig. 9 was found to directly affect the motion of the Ch droplets. The droplet in Figs. 9(b1) and 9(b2) performing Brownian motion in the equilibrium exhibited continuous rotation under a temperature gradient. On the other hand, the droplet with surface contact with the upper substrate exhibited neither thermal fluctuation nor rotation, even under a large temperature gradient. Although the glass substrates were carefully cleaned, as beforementioned, it was difficult to obtain a perfectly uniform hydrophilic surface. The adhesion of the droplets to the substrate surface significantly disturbed their motion, which is supposed to be the main reason why the Ch droplets had never rotated in glycerol in the previous studies.

3.5 *Estimate of the coupling constant*

Confirming the rigid body rotation of the Ch droplets and the linear relation between the angular velocity ω and the temperature gradient ∇T, we can estimate the thermomechanical coupling constant ν given in Eq. (1). As shown in Fig. 7, $\omega/|\nabla T|$ depended on the droplet size, so let us use the moderate value of $\omega/|\nabla T| \sim 4 \times 10^{-3}$ (rad s^{-1})/(K μm^{-1}) as a representative. When a droplet rotates as a rigid body, the total torque on the whole droplet should be given by the volume integral of Eq. (1). Substituting the director field Ansatz of RSS given by Bezić and Žumer as[13] $\boldsymbol{n} = \cos\Omega\mathbf{e}_\theta + \sin\Omega\mathbf{e}_\varphi$ with $\Omega = \varphi + 2\pi r/P$, where P is the cholesteric pitch to Eq. (1), we can calculate the thermomechanical torque exerted on an RSS droplet when the temperature gradient is parallel to the symmetry axis ($\nabla T = |\nabla T|\boldsymbol{e}_z$), resulting in

$$\begin{aligned}\boldsymbol{\Gamma} &= \nu|\nabla T| \int \boldsymbol{n} \times (\boldsymbol{n} \times (-\boldsymbol{e}_z))\, dV \\ &= \nu|\nabla T|\mathbf{e}_z \int (\cos^2\Omega\cos^2\theta + \sin^2\Omega)\, dV = \nu\frac{8\pi R^3}{9}\nabla T,\end{aligned} \tag{2}$$

where R is the droplet radius. This active thermomechanical torque should be balanced with the viscous torque when the droplet rotates at a constant angular velocity ω in glycerol with viscosity η. For simplicity, let us substitute the well-known formula of $8\pi\eta R^3\omega$ as the lower limit[24] for the viscous torque, resulting in

$$\left|\nu\frac{8\pi R^3}{9}(\nabla T)_z\right| \geq 8\pi\eta R^3|\omega|. \tag{3}$$

Substituting $(\nabla T)_z = 10\,\mathrm{mK\,\mu m^{-1}}$, $\omega = 4 \times 10^{-3}\,\mathrm{rad\,s^{-1}}$, and $\eta = 0.08\,\mathrm{Pa\,s}$ (the viscosity of glycerol at $T \sim 60\,^\circ\mathrm{C}$) into Eq. (2), we obtain $|\nu| \geq 3 \times 10^{-7}\,\mathrm{N\,m^{-1}\,K^{-1}}$. In the previous studies, the coupling constants for the Ch droplets coexisting with the isotropic phase were given as[2,25,26] $(1–4) \times 10^{-6}$ $\mathrm{N\,m^{-1}\,K^{-1}}$. It turned out that the Ch droplets dispersed in glycerol can unidirectionally rotate under the temperature gradient at a comparable efficiency to that for the droplets coexisting with their isotropic phase.

4. Conclusion

Dispersing micron-sized Ch droplets in glycerol and applying a uniform temperature gradient to the emulsions, we demonstrated the steady unidirectional rotation of the Ch droplets driven by a heat flux. This is in clear contrast to the previous studies showing that the Ch droplets, even subjected to a temperature gradient, never rotated in immiscible liquids. The rotational direction was reversed by inversing either the chirality of the dopants or the temperature gradient sign, and the rotational velocity was linear to the temperature gradient magnitude. All these properties agreed well with Leslie's phenomenological model. By the PTV method, we found that the droplet rotated as a rigid body without either Marangoni convection or mass fluxes, which indicates that the heat flux should purely drive the steady rotation of the droplets. The thermomechanical coupling constant, i.e., the conversion

efficiency from the heat flux to the torque, was roughly estimated as $|\nu| \geq 3 \times 10^{-7}\,\mathrm{N\,m^{-1}\,K^{-1}}$. This is comparable to the Ch droplets coexisting with their isotropic phase. The hydrophilicity of the substrate surface is crucial to rotating the Ch droplets in glycerol. On the highly hydrophilic clean surface, the glycerol molecules were absorbed, which resulted in playing the role of lubricant as well as disturbing the adhesion of the Ch droplets. Whether being dispersed in immiscible liquids or coexisting with the isotropic phase, the Ch droplets under a temperature gradient should be subjected to the thermomechanical torque and are possible to exhibit steady unidirectional rotation.

Acknowledgment This work was supported by Grant-in-Aid for Scientific Research B (22H01422).

*tabe@waseda.jp

1) O. Lehmann, Ann. Phys. **307**, 649 (1900).
2) P. Oswald and A. Dequidt, Phys. Rev. Lett. **100**, 217802 (2008).
3) P. Oswald, Eur. Phys. J. E **28**, 377 (2009).
4) J. Yoshioka, F. Ito, Y. Suzuki, H. Takahashi, H. Takizawa, and Y. Tabe, Soft Matter **10**, 5869 (2014).
5) K. Nishiyama, S. Bono, Y. Maruyama, and Y. Tabe, J. Phys. Soc. Jpn. **88**, 063601 (2019).
6) S. Bono, Y. Maruyama, and Y. Tabe, Soft Matter **14**, 9798 (2018).
7) J. Yoshioka and F. Araoka, Nat. Commun. **9**, 432 (2018).
8) P. Oswald, J. Ignés-Mullol, and A. Dequidt, Soft Matter **15**, 2591 (2019).
9) J. Yoshioka and F. Araoka, Sci. Rep. **10**, 17226 (2020).
10) P. Oswald, A. Dequidt, and G. Poy, Liq. Cryst. Rev. **7**, 142 (2019).
11) F. M. Leslie, Proc. R. Soc. A **307**, 359 (1968).
12) D. Seč, T. Porenta, M. Ravnik, and S. Žumer, Soft Matter **8**, 11982 (2012).
13) J. Bezić and S. Žumer, Liq. Cryst. **11**, 593 (1992).
14) (Supplemental Material) MOVIE 2a_x 900.avi, corresponding to Fig. 2(a), is provided online. The movie is played at 900 times as fast as the real speed, showing the RSS droplet with (R)-dopant subjected to the temperature gradient of $+10.0\,\mathrm{mK\,\mu m^{-1}}$.
15) (Supplemental Material) MOVIE 2b_x 900.avi, corresponding to Fig. 2(b), is provided online played at 900 times as fast as the real speed. The droplets with (S)-dopant subjected to the temperature gradient of $+20.0\,\mathrm{mK\,\mu m^{-1}}$.
16) (Supplemental Material) MOVIE 2c_x 900.avi, corresponding to Fig. 2(c), is provided online, which is played at 900 times as fast as the real speed. The droplets with (R)-dopant subjected to the temperature gradient of $-20.0\,\mathrm{mK\,\mu m^{-1}}$.
17) (Supplemental Material) MOVIE 5a_x 900.avi, corresponding to the upper left sequential images in Fig. 5, is provided online, played at 900 times as fast as the real speed. The RSS droplet with (R)-dopant subjected to the temperature gradient of $+10.0\,\mathrm{mK\,\mu m^{-1}}$.
18) (Supplemental Material) MOVIE 5b_x 900.avi, corresponding to the lower left sequential images in Fig. 5, is provided online, played at 900 times as fast as the real speed. The RSS droplet with (R)-dopant subjected to the temperature gradient of $-10.0\,\mathrm{mK\,\mu m^{-1}}$.
19) (Supplemental Material) MOVIE 5c_x 900.avi, corresponding to the upper right sequential images in Fig. 5, is provided online, played at 900 times as fast as the real speed. The RSS droplet with (S)-dopant subjected to the temperature gradient of $+10.0\,\mathrm{mK\,\mu m^{-1}}$.
20) (Supplemental Material) MOVIE 5d_x 900.avi, corresponding to the lower right sequential images in Fig. 5, is provided online, played at 900 times as fast as the real speed. The RSS droplet with (S)-dopant subjected to the temperature gradient of $-10.0\,\mathrm{mK\,\mu m^{-1}}$.
21) (Supplemental Material) MOVIE 8a_x 2700.avi, corresponding to Fig. 8(a), is provided online, played at 2700 times as fast as the real speed. The RSS droplet containing (R)-dopant with the marker particle under $\nabla T = +20.0\,\mathrm{mK\,\mu m^{-1}}$.
22) (Supplemental Material) MOVIE 8b_x 2700.avi, corresponding to Fig. 8(b), is provided online, played at 2700 times as fast as the real speed. The RSS droplet containing (R)-dopant with the marker particle under $\nabla T = +10.0\,\mathrm{mK\,\mu m^{-1}}$.
23) (Supplemental Material) MOVIE 8c_x 2700.avi, corresponding to Fig. 8(c), is provided online, played at 2700 times as fast as the real speed. The RSS droplet containing (S)-dopant with the marker particle under $\nabla T = +20.0\,\mathrm{mK\,\mu m^{-1}}$.
24) Since the droplets exist in the vicinity of the substrate, the viscous torque should be larger than the value when a hard sphere is rotating in an infinite viscous fluid.
25) S. Bono, Y. Maruyama, K. Nishiyama, and Y. Tabe, Eur. Phys. J. E **42**, 99 (2019).
26) K. Nishiyama, S. Bono, and Y. Tabe, Soft Matter **17**, 10818 (2021).